

Serveur Académique Lausannois SERVAL serval.unil.ch

Author Manuscript

Faculty of Biology and Medicine Publication

This paper has been peer-reviewed but does not include the final publisher proof-corrections or journal pagination.

Published in final edited form as:

Title: Quantification of brain glycogen concentration and turnover through localized ¹³C NMR of both the C1 and C6 resonances.

Authors: van Heeswijk RB, Morgenthaler FD, Xin L, Gruetter R

Journal: NMR in biomedicine

Year: 2010 Apr

Issue: 23

Volume: 3

Pages: 270-6

DOI: 10.1002/nbm.1460

In the absence of a copyright statement, users should assume that standard copyright protection applies, unless the article contains an explicit statement to the contrary. In case of doubt, contact the journal publisher to verify the copyright status of an article.

Quantification of brain glycogen concentration and turnover through localized ^{13}C NMR of both the C1 and C6 resonance

Ruud B. van Heeswijk¹, Florence D. Morgenthaler¹, Lijing Xin¹ and Rolf Gruetter^{1,2,3}

¹Laboratory for Functional and Metabolic Imaging, EPFL, Lausanne, Switzerland; ²Department of Radiology, University of Lausanne, Lausanne, Switzerland; and ³Department of Radiology, University of Geneva, Geneva, Switzerland

Address for correspondence:

Rolf Gruetter

Centre d'Imagerie BioMedicale (CIBM)

CH F1 542, Station 6

Ecole Polytechnique Fédérale de Lausanne (EPFL)

1015 Lausanne, Switzerland

Tel: +41-21-6934467

Fax: +41-21-6937960

E-mail: Rolf.Gruetter@epfl.ch

Keywords: glycogen, turnover, Fourier series window

Abbreviations used: NAA, FSW, NMR, Glyc, Glc, IE, VOI, FOV

Abstract

We have recently shown that at isotopic steady state ^{13}C NMR can provide a direct measurement of glycogen concentration changes, but that the turnover of glycogen was not accessible with this protocol. The aim of the present study was to design, implement and apply a novel dual-tracer infusion protocol to simultaneously measure glycogen concentration and turnover. After reaching isotopic steady state for glycogen C1 using $[1\text{-}^{13}\text{C}]$ glucose administration, $[1,6\text{-}^{13}\text{C}_2]$ glucose was infused such that isotopic steady state was maintained at the C1 position, but the C6 position reflected ^{13}C label incorporation. To overcome the large chemical shift displacement error between the C1 and C6 resonances of glycogen, we implemented 2D gradient based localization using the Fourier series window approach, in conjunction with time-domain analysis of the resulting FIDs using jMRUI. The glycogen concentration of 5.1 ± 1.6 mM measured from the C1 position was in excellent agreement with concomitant biochemical determinations. Glycogen turnover measured from the rate of label incorporation into the C6 position of glycogen in the α -chloralose anesthetized rat was $0.7 \mu\text{mol/g/h}$.

Introduction

Glycogen (Glyc) is a macromolecule consisting of linked glycosyl units that serves as a storage molecule for glucose (Glc) in the body. Since it has a much lower concentration in the brain than in tissues such as muscle and the liver, its role as a cerebral energy store has been largely neglected, although over the last decade interest has been renewed for several reasons: not only does it appear play an active role in brain energy homeostasis (1), it is also involved in such processes as memory formation (2) and neurotransmitter synthesis (3). Additionally, it has been implicated in hypoglycemia unawareness, a dangerous complication often encountered in patients treated with exogenous insulin (4).

Glycogen concentrations are the result of the simultaneous action of its synthesis and catalysis (i.e. turnover), resulting in a well-regulated level of brain glycogen in the resting state. In order to gain insight into the role of glycogen in the abovementioned processes, it is important to determine concentration and metabolic rates.

Metabolism of glycogen can be assessed by measuring the incorporation of its precursor glucose that has been labeled with an isotope like ^{13}C , ^3H or ^{14}C . From the time or rate of label incorporation, turnover times or rates can be determined. Currently, the only method to measure label incorporation into glycogen non-invasively *in vivo* is ^{13}C nuclear magnetic resonance (NMR)(1). Following the infusion of 99% isotopically enriched (IE) $[1-^{13}\text{C}_1]$ Glc, incorporation of ^{13}C label into Glyc can be measured (5). However, such measurements of ^{13}C label incorporation may be due to increased Glyc IE or due to a net increase in Glyc concentration.

We have previously shown that the absolute concentration of brain Glyc can be determined from the C1 resonance by 'prelabeling' with $[1-^{13}\text{C}]$ Glc, i.e. providing the animal exclusively with food that only contains $[1-^{13}\text{C}]$ Glc as a source of carbon prior to the experiment (6): when the enrichment at C1 reached steady state, the IE of N-acetylaspartate (NAA) was used to determine the IE of Glyc *in vivo*. This approach allowed the measurement of the Glyc concentration, but provided no information on turnover.

However, if after this prelabeling $[1,6-^{13}\text{C}_2]$ Glc is infused at the IE of the Glyc C1 resonance, the C1 resonance will remain in isotopic steady state and will act as a pure concentration change monitor, while the C6 resonance signal will increase mostly due to label incorporation, and can in principle be monitored to determine the turnover time. The aim of the present study was therefore to establish the simultaneous measurement of the glycogen C1 and C6 resonances, such that the C1 resonance can be used to determine concentration and the C6 resonance can be used to determine the turnover time.

One of the challenges of measuring the Glyc C1 and C6 resonances simultaneously is that they are separated by ~4 kHz at 9.4 T due to their chemical shifts of 100.5 and 61.4 ppm respectively. Such a large frequency difference represents a formidable challenge for 3D spatial localization using gradient-based methods, to date the only method capable of measuring NMR of Glyc in the brain. To overcome chemical shift displacement (CSD), one of the goals of the present study was therefore to implement a new gradient-based localization sequence that aimed to minimize CSD: the two-dimensional Fourier series window (FSW, (7)).

Fourier series window (FSW) based pulse sequences have been used mostly for ^{31}P NMR in muscle and liver (8-10). The FSW is an alternative to traditional Fourier transform chemical shift imaging (CSI). A predetermined voxel shape is chosen for which a single window W (the voxel) of resolution N is generated by summation of $2N+1$ phase-encoded FIDs that are multiplied by a series of matching Fourier coefficients β_n (see appendix A for a recapitulation of FSW theory).

The FSW localization approach can be tailored to achieve arbitrary voxel shapes, has low cross-voxel contamination and a complete lack of chemical shift displacement (11). The number of repetitions per phase encoded FID should correspond to the Fourier coefficient's relative weight; a phase encode with a low Fourier coefficient will need only a few averages, while a high coefficient should imply many averages for efficient performance. The FSW approach is thus ideally suited for applications that require many averages as is the case for ^{13}C NMR of glycogen.

Therefore the aim of the present study was two-fold: first to implement a localization scheme based on the 2D Fourier series window to minimize chemical shift displacement, and second to establish a dual-isotope protocol using $[1,6-^{13}\text{C}_2]$ glucose and to determine the glycogen turnover time while monitoring its concentration.

Methods

NMR instrumentation

All experiments were performed using an actively shielded 9.4 T 31 cm horizontal-bore Varian spectrometer with high-performance gradients (400 mT/m in 130 μ s). A custom-built 3-loop 10 mm diameter surface coil was used for ^{13}C excitation and detection, while quadrature 14 mm ^1H coils were used for positioning, shimming and decoupling (12). Shimming was performed with FASTMAP (13).

FSW pulse sequence

The total delay for the gradients to play out between the excitation pulse and the start of the acquisition was 270 μ s (Fig. 1), which should result in less than 3% signal loss due to the estimated glycogen T_2 of 10 ms (14). Slice selection in the third dimension was achieved using one-dimensional ISIS (15), using a 6 ms hyperbolic secant pulse to select a slice of 1 cm thickness. A minimum of two averages was thus required per gradient setting. We propose the acronym FOSSIL (FOurier Series-based Spectroscopic Imaging Localization) for this 2D FSW-based pulse sequence.

WALTZ-16 broadband NOE and decoupling were applied at the ^1H water frequency (16). A 3 ms 90° BIR-4 pulse (17) was used for excitation, with a nominal bandwidth of 5 kHz at 2.5 kHz $\gamma B_{1\text{max}}$, sufficient to cover the 3.9 kHz frequency difference between the Glyc C1 and C6 resonances (Fig. 2). The BIR-4 pulse has a semi-linear phase variation that increasingly varies near the edges of its nominal bandwidth.

The Fourier coefficients were calculated (see appendix) for a square two-dimensional Fourier series window in two dimensions with a field of view (FOV) of 22 x 22 mm^2 . For a window resolution of 1/5 FOV (4.4x4.4 mm^2) and N=5 coefficients this resulted in $(2N+1)^2=121$ phase encodes, while for 1/8 FOV (2.75x2.75 mm^2) and N=8 coefficients it resulted in 289 phase encodes. Each of these phase encodes had its number of acquisitions adapted to its 2D Fourier coefficient θ_n (Eq. A.5 in the appendix).

Validation of FSW localization in phantom experiments

To verify the localization accuracy of the FSW sequence, we used a seven-compartment phantom, consisting of a water-filled Perspex half-cylinder in which 6 tubes with different solutions were mounted. The tubes contained saturated solutions of either bicarbonate (of which the carboxyl carbon resonates at 168.9 ppm), formate (174.0 ppm), carbonate (161.1 ppm) or acetate (182.2 ppm).

To account for the long T_1 relaxation time of the carboxyl groups (6-30 s) the repetition time was 10 s. The average number of acquisitions per gradient setting was 12, adjusted according to the relative coefficient weight (see appendix).

***In vivo* measurements**

To determine the brain Glyc turnover rates and concentrations, six Sprague-Dawley rats (~225 g, Charles River Laboratories, France) were fasted overnight (Fig. 3). The next morning, for 24 hours before the start of the NMR experiments, they were fed 100% enriched, 10% w/v [$1\text{-}^{13}\text{C}_1$] Glc in tap water ad libitum to achieve isotopic steady state for the Glyc C1 resonance as described previously (6).

On the day of the NMR measurement, the animal was anesthetized with 2% isoflurane. Both femoral veins and a femoral artery were catheterized for infusion of glucose and α -chloralose, and blood-gas analysis respectively. After surgery, anesthesia was switched to α -chloralose (an initial bolus of 80mg/kg followed by continuous infusion of 50mg/kg/h with 5mg/ml α -chloralose in saline) under assisted breathing, and the animal was placed in the NMR scanner where its temperature was kept at 37.5 ± 0.5 °C with circulating warm water. While the animal was in the scanner, blood samples were taken for blood-gas and glycemia analysis every 30 min to monitor physiology.

Glycogen NMR studies

Two sets of 'baseline' datasets with the FSW-based sequence were acquired to determine the glycogen

and glucose levels at steady state. With a repetition time of 1 s, averaging of the phase encodes at 5 coefficients per dimension for a 1/5 FOV window (see appendix) was calculated such that the total acquisition time was 59 min (see appendix). The ^{13}C carrier frequency was placed in the center of the Glyc C1 and C6 resonances, while broadband decoupling was applied at the Glc ^1H frequency.

After these baseline acquisitions, a bolus of 0.6 mg/kg $[1,6-^{13}\text{C}_2]$ Glc whose IE matched that of Glyc C1 was given over 5 min, and a variable-rate infusion of $[1,6-^{13}\text{C}_2]$ Glc was used afterwards to maintain blood Glc level at 10 mM. Seven more 5x5 FSW datasets were then acquired with a temporal resolution of 1 h.

After the study, the animal was sacrificed using 2 s of focused 4 kW microwave radiation (Gerling Applied Engineering, Modesto, CA). The brain was taken out and stored at $-80\text{ }^\circ\text{C}$ for later biochemical determination of Glyc content and high resolution NMR determination of Glyc IE.

A phantom containing 500 mM Glyc (Sigma-Aldrich, St. Louis, MO) and 5 mM $[1-^{13}\text{C}]$ Glc was then placed under the coil at $T = 37\text{ }^\circ\text{C}$, and another set of 5x5 FSW was acquired for absolute quantification purposes as described previously (6).

Isotopic enrichment

The IE of the steady state Glyc C1 position was determined *in vivo* to match the IE of infused Glc to this IE and thus to keep the Glyc C1 IE constant. Since the steady state IE of glycogen using this protocol is 2.2 times that of N-acetylaspartate (NAA) (6), the NAA IE was determined by comparing the ^{13}C -coupled ^1H NAA doublet signals to that of the ^{12}C -coupled ^1H NAA singlet in a modified ACED-STEAM (18) sequence as described previously (6).

Brain extract measurements

The extracted brains were homogenized and prepared for Glc concentration measurement as well as

verification of the IE as previously described (19). Briefly, after powderizing the brain by mortar and pestle, 200 μ l of 0.03 M sodium acetate was added, which was then homogenized with an ultrasonic processor. The sample was divided into two aliquots, one of which was incubated at 37 °C with α -1,4- α -1,6-glucosidase, while the other was incubated with a saline solution. From the glucose content measured in a glucose analyzer (GM7 Micro-stat, Analox Instruments, London, UK), one aliquot effectively gave the summed glucose and glycogen concentration, while the other gave the free tissue glucose concentration. After filtering, lyophilizing and resuspension in D₂O, high-resolution ¹H NMR spectra of these samples were obtained at 600 MHz. The ratio of the ¹³C bound doublet and ¹²C-bound singlet were used to calculate the IE of free glucose in one aliquot, and the concentration-weighted average IE of Glc and Glyc in the other. The free glucose IE was then used to calculate the Glyc IE from the concentration-weighted average IE of Glc and Glyc using Eq. 3 from Ref. (6).

Spectral processing

The calculation of the localized FIDs from the coefficient weighted individual FSW FIDs was done in MATLAB (The Mathworks Inc., Natick, MA, USA) using Eq. A.3 in the appendix. The datasets were reconstructed into a grid of 16x16 to allow the selection of an optimally positioned voxel for every study. The resulting FIDs were subsequently DC corrected and multiplied with a 15 Hz exponential decay.

The localized FIDs were processed in the time-domain using the jMRUI software package (20,21). A frequency filter was applied to select the chemical shift range from 47 to 110 ppm. A total of 10 signal components were fitted using AMARES (Advanced Method for Accurate, Robust, and Efficient Spectral fitting) (22): Glyc C1, Glc C1 β , Glc C1 α , glycerol C1, Glc C6, Glyc C6, a peak each for glutamine C2, glutamate C2 and aspartate C2, plus a term accounting for any residual DC offset. The linewidths of glucose (C1 α , C1 β and C6) were constrained to be equal, and the linewidths of Glyc C1 and C6 were

constrained to be equal. These constraints on Glyc C6 and Glc C6 allowed to separately quantify the overlapping C6 resonances of Glc and Glyc. Since the phase of each individual resonance was stable throughout the experiment, the phase was estimated for each animal from the summed time series; the phase however varied along the spectrum due to the phase profile of the BIR-4 excitation pulse (Fig. 2a). To minimize the influence of the broad baseline components, the first 10 data points of the signals were weighted with a quarter-sine wave (22).

Quantitation and turnover calculation

Absolute concentrations of Glc C1, Glyc C1 and Glyc C6 were calculated from the *in vivo* and phantom signals S , the signals of the formic acid reference phantom in both situations (to correct for RF loading) and a correction factor α for differences in NOE and partial T_1 relaxation as in previous studies ((23) and references therein). This results in:

$$[Gl]_{iv} = \frac{S_{Gl,iv}}{S_{Gl,ph}} \frac{S_{FA,iv}}{S_{FA,ph}} \alpha \frac{1.1\%}{IE_{Gl,iv}} [Gl]_{ph} \cdot \quad (1)$$

Here the Gl and FA are glucose/glycogen and formic acid, while iv and ph are *in vivo* and phantom.

OriginPro (OriginLab Corporation, Northampton, MA, USA) was used to fit the concentration time courses. Glyc C6 was fitted with an exponential increase ($C(t)=[Glyc]_{C6} \cdot \exp[-t/\tau]$), while the Glc C1 and Glyc C1 time courses were fitted with constants, as there was no time dependence discernible.

Results

The localization ability of the 2D FSW sequence was tested on a phantom containing bicarbonate, formate, carbonate and acetate (Fig. 4). Despite the range of 20 ppm in chemical shift, the FSW signals of a formate, carbonate and acetate compartment overlap with their 1H image equivalents, as evidenced from the FSW color maps of the resonances projected on top of a 1H gradient echo image (Fig. 4b). Note

that the compartments that were more than ~10 mm away from the surface coil plane were outside the sensitive volume of the small ^{13}C coil and thus not detected.

Localization of the 2D FSW sequence was further tested *in vivo*. Since it is well established that ^{13}C resonances from lipids originate outside the brain, good localization should eliminate lipid-specific resonances. When placing the voxel of interest (VOI) into superficial regions encompassing fat and muscle, clearly resonances ascribed to extra-cerebral fat (glycerol C1,3 at 62.5 ppm) were detected (Fig. 5b). Moving the VOI into the brain minimized the glycerol resonance (Fig. 5c).

The bandwidth of the BIR-4 pulse was ~5 kHz, sufficient to simultaneously excite the Glyc C1 and C6 resonance with less than 10% signal loss, according to simulations (Fig. 2) and verified in phantom studies. Since the RF coil's RF loading varied per subject, the effective power for the 90° BIR-4 RF pulse was varied slightly each time, causing the zero and first order phase of the spectra to vary slightly from study to study, as expected from the pulse profile (Fig. 2b). Therefore, while the magnitude of the excited signal for the resonances of interest was comparable across all studies, the phase over the entire spectrum varied up to 70° . Especially the phase of the Glyc C1 and Glyc/Glc C6 resonances, while stable per subject, showed large variations across subjects. Nonetheless, the signal-to-noise ratio of the localized spectra was in all cases high enough to allow robust fitting using the time-domain AMARES fitting routine, including the aforementioned phase variations, resulting in negligible residuals over the spectral regime of interest (Fig. 6).

The time courses of the Glyc and Glc C1 signal were within experimental error constant, consistent with the isotopic steady-state achieved using this protocol (Fig. 7). For the quantitation, both C1 resonances were corrected for the IE (measured from NAA as in our previous study), which was established at $IE_{\text{Glyc,inv}} = 42 \pm 6\%$. The *in vivo* IE determination was within a few percent comparable to

that in brain extracts (as previously, (6)): a linear fit through the origin resulted in

$$IE_{\text{Glyc,invivo}}=1.03 \cdot IE_{\text{Glyc,highres}} \quad (R^2=0.98, P=0.16).$$

From the thus determined IE of Glyc and the $[1-^{13}\text{C}]$ Glyc concentration measured by *in vivo* NMR, the total concentration of glycogen and glucose was calculated using Eq. 1, resulting in total Glc and Glyc concentrations of $[\text{Glc}]_{t,C1} = 4.3 \pm 1.0$ and $[\text{Glyc}]_{t,C1} = 5.1 \pm 1.6$ mM respectively. Here the subscript t stands for total, while C1 indicates that the concentration was based on the integral of the C1 resonance. The determined glycogen concentrations were within experimental error identical to that determined by concomitant biochemical assays, which yielded $[\text{Glyc}]_{t,\text{assay}} = 5.3 \pm 1.6$ mM.

The Glc C6 signal increased in a step-like manner to reach steady state levels within 30 min after the start of the $[1,6-^{13}\text{C}_2]$ Glc infusion at $t = 0$, whereas the Glyc C6 signal slowly increased over time. Given that the stability of Glyc C1 indicated minimal concentration changes, this gradual increase in the Glyc C6 signal therefore mainly represents changes in the IE of Glyc C6, and thus can be used to estimate glycogen turnover time. An exponential fit of the Glyc C6 signal with $C(t) = [\text{Glyc}]_{C6} \cdot \exp(-t/\tau)$ resulted in a turnover time of 8 ± 4 h ($R^2 = 0.97$) and a steady state Glyc C6 concentration of $[\text{Glyc}]_{C6} = 3 \pm 1$ mM. Dividing the steady state concentration of the Glyc C6 time course by its IE (assuming the same C6 IE at steady state as the C1 resonance) resulted in a total glycogen concentration $[\text{Glyc}]_{t,C6} = 7 \pm 3$ mM. By dividing the average $[\text{Glyc}]_t$ by τ we calculated a Glyc turnover rate of 0.7 ± 0.6 $\mu\text{mol/g/h}$.

Discussion

In this study we implemented and used the Fourier series window approach for the first time for 2D localization of ^{13}C signals, which, combined with a novel dual isotope infusion protocol, allowed the simultaneous determination of glycogen concentration and turnover.

While the dephasing that the phase encoding generates implies that the 2D FSW pulse sequence is theoretically not as efficient as single-voxel localized spectroscopy, the sequence does have the same efficiency equivalent to conventional spectroscopic imaging, provided that the amount of acquisitions per gradient setting are weighted by their Fourier coefficient. Therefore, the SNR per time unit observed in the present study was ~70% that of single-voxel ^{13}C spectroscopy studies (6,16). The sequence appears to be a suitable alternative for regular spectroscopic imaging or localized spectroscopy if large chemical shift ranges are to be localized, provided sufficient averaging is performed.

Time-domain fitting of the spectra was robust: the phase variations across the chemical shift of the FSW spectra were expected from the simulations of the BIR-4 pulse and were easily accounted for by the AMARES routine. The step-like increase of Glc C6 at the start of the infusion together with the slow increase of Glyc C6 over time indicated that their resonances were robustly deconvolved based on their substantially different linewidths, despite Glyc and Glc C6 having considerable spectral overlap.

The 2D FSW pulse sequence was combined with the isotopic enrichment (IE) determination and external reference quantification to obtain absolute quantifications of Glyc. IE determination was in excellent agreement with previous results (6,23), and the *in vitro* biochemistry and high resolution ^1H NMR confirmed the validity of the *in vivo* method.

The absolute quantification of the C1 resonance resulted in total Glc and Glyc concentration time that were constant over time, indicating stable Glyc and Glc concentrations, the former validated by biochemical *in vitro* analysis and in agreement with previously reported levels under similar hyperglycemic and anesthetic conditions (19). Due to the slightly hyperglycemic level at which the blood glucose was maintained, a slight increase in the Glyc concentration over time could also have been expected. This was however not observed, which may be due to SNR being too low to detect such a small increase: a linear Glyc C1 time course fit in which the slope was left free resulted in a slope of -

$8 \times 10^{-4} \pm 0.25$ mM/h, showing that a glycogen concentration increase of at least 0.5 mM/h was necessary to be statistically significant.

Conclusions

We conclude that a) Glyc C1 and C6 can be simultaneously measured *in vivo* using the Fourier series window based pulse sequence, and that b) the dual isotope infusion protocol proposed can be used to simultaneously determine both the glycogen concentration and turnover *in vivo*.

Appendix: FSW theory and calculations

The Fourier series window approach has in NMR mostly been used for ^{31}P spectroscopic imaging. A more in-depth treatment of the theoretical background can be found in Refs (7,9,11,24). For convenience, a short overview of this theory is given in this appendix.

In a one-dimensional FSW pulse sequence a predetermined window shape W (the voxel) is chosen with a resolution N and window width FOV/N . A phase encoding gradient is applied to the transverse magnetization such that distance becomes equivalent to the phase φ . The window itself can then be described as a set of $2N+1$ Fourier coefficients β_n such that in the one-dimensional case it looks like (7):

$$W(\varphi) = \sum_{-N}^N \beta_n e^{in\varphi} . \quad (\text{A.1})$$

To determine the coefficients β_n , one can reverse Eq. 1 and integrate from $-\pi$ to π :

$$\beta_n = \frac{1}{2\pi} \int d\varphi W(\varphi) e^{-in\varphi} . \quad (\text{A.2})$$

To not repeat the window inside the field of view (FOV), the first coefficient β_1 is set to have an accompanying phase encoding step which has a phase spread of 180° over the FOV. When applied to the spatially encoded MR signal $\rho(\vec{r}, t)$, the window is convolved with a series of phase-encoded FIDs $S(n, t)$:

$$\int d\vec{r} \rho(\vec{r}, t) W(\varphi) = \sum_{-N}^N \beta_n S(n, t). \quad (\text{A.3})$$

The window can be arbitrarily shifted a distance ψ by multiplying the window with $e^{-in\psi}$ (i.e. Fourier shifting). The windowed spatially encoded time-domain signal is now:

$$\int d\vec{r} \rho(\vec{r}, t) W(\varphi + \psi) = \int d\vec{r} \rho(\vec{r}, t) \left[\sum_{-N}^N \beta_n e^{in(\psi + \varphi)} \right] = \sum_{-N}^N \beta_n S(n, t) e^{in(\psi)}. \quad (\text{A.4})$$

With these equations the parameters for the window of choice can be calculated. In these studies, a square window shape was chosen, so Eq. 2 was solved for the square shape with width w , resulting in 1D coefficients β_n :

$$\beta_n = \frac{\sin(nw/2)}{n\pi}. \quad n = -N, -N+1, \dots, 0, \dots, N-1, N \quad (\text{A.5})$$

The $2N+1$ coefficients for the phase encoding combinations can now be calculated. N is usually chosen such that the resolution is FOV/N . The resulting voxel is only approximately rectangular due to truncation by the finite number of coefficients. However, terminating the coefficient function of Eq. 4 at the first zero crossing (i.e. where $n = \pm 2\pi/w$) substantially reduces any truncation effects(24). The shape of the window results in a slightly larger area than its nominal width, yet 99% of the window intensity drops off at 1.4 times the window width. The 2D FSW separately applies the above equations to the second dimension coefficients β_m as well, resulting in $(2N+1)^2$ doubly weighted phase encodes.

Acknowledgements

The authors would like to thank Dr. Paul Vasos for his help with the high resolution spectrometer, and Ms. Hanne Frenkel and Dr. Agathe Python for their veterinary assistance. Supported by Centre d'Imagerie BioMédicale (CIBM) of the UNIL, UNIGE, HUG, CHUV, EPFL and the Leenaards and Jeantet Foundations; NIH grant R01NS42005 and SNSF grant 3100A0-122498.

References

1. Gruetter R. Glycogen: the forgotten cerebral energy store. *J Neurosci Res* 2003;74(2):179-183.
2. Gibbs ME, Anderson DG, Hertz L. Inhibition of glycogenolysis in astrocytes interrupts memory consolidation in young chickens. *Glia* 2006;54(3):214-222.
3. Brown AM, Sickmann HM, Fosgerau K, Lund TM, Schousboe A, Waagepetersen HS, Ransom BR. Astrocyte glycogen metabolism is required for neural activity during aglycemia or intense stimulation in mouse white matter. *J Neurosci Res* 2005;79(1-2):74-80.
4. Cryer PE. Mechanisms of hypoglycemia-associated autonomic failure and its component syndromes in diabetes. *Diabetes* 2005;54(12):3592-3601.
5. Choi IY, Gruetter R. In vivo ¹³C NMR assessment of brain glycogen concentration and turnover in the awake rat. *Neurochem Int* 2003;43(4-5):317-322.
6. Morgenthaler FD, van Heeswijk RB, Xin L, Laus S, Frenkel H, Lei H, Gruetter R. Non-invasive quantification of brain glycogen absolute concentration. *J Neurochem* 2008;107(5):1414-1423.
7. Garwood M, Schleich T, Ross BD, Matson GB, Winters WD. A Modified Rotating Frame Experiment Based on a Fourier-Series Window Function - Application to In vivo Spatially Localized Nmr-Spectroscopy. *Journal of Magnetic Resonance* 1985;65(2):239-251.
8. Garwood M, Schleich T. Improved fourier series windows for localization in in vivo NMR spectroscopy. *J Magn Reson* 1985;65:510-515.
9. Hendrich K, Merkle H, Weisdorf S, Vine W, Garwood M, Ugurbil K. Phase-Modulated Rotating-Frame Spectroscopic Localization Using an Adiabatic Plane-Rotation Pulse and a Single Surface Coil. *Journal of Magnetic Resonance* 1991;92(2):258-275.
10. Garwood M, Ugurbil K, Schleich T, Sublett E, From A. In vivo spatially localized surface-coil NMR spectroscopy utilizing a fourier series window function and two surface coils. *J Magn Reson* 1986;69:576-581.
11. Hendrich K, Hu XP, Menon RS, Merkle H, Camarata P, Heros R, Ugurbil K. Spectroscopic Imaging of Circular Voxels with a 2-Dimensional Fourier-Series Window Technique. *Journal of Magnetic Resonance Series B* 1994;105(3):225-232.
12. Adriany G, Gruetter R. A half-volume coil for efficient proton decoupling in humans at 4 tesla. *J Magn Reson* 1997;125(1):178-184.
13. Gruetter R. Automatic, localized in vivo adjustment of all first- and second-order shim coils. *Magn Reson Med* 1993;29(6):804-811.
14. Overloop K, Vanstapel F, Van Hecke P. ¹³C-NMR relaxation in glycogen. *Magn Reson Med* 1996;36(1):45-51.

15. Ordidge RJ, Connelly A, Lohman JAB. Image-Selected In vivo Spectroscopy (Isis) - a New Technique for Spatially Selective Nmr-Spectroscopy. *Journal of Magnetic Resonance* 1986;66(2):283-294.
16. Choi IY, Tkac I, Gruetter R. Single-shot, three-dimensional "non-echo" localization method for in vivo NMR spectroscopy. *Magn Reson Med* 2000;44(3):387-394.
17. Garwood M, Yong K. Symmetrical Pulses to Induce Arbitrary Flip Angles with Compensation for Rf Inhomogeneity and Resonance Offsets. *Journal of Magnetic Resonance* 1991;94(3):511-525.
18. Frahm J, Merboldt KD, Hanicke W. Localized Proton Spectroscopy Using Stimulated Echoes. *Journal of Magnetic Resonance* 1987;72(3):502-508.
19. Morgenthaler FD, Koski DM, Kraftsik R, Henry PG, Gruetter R. Biochemical quantification of total brain glycogen concentration in rats under different glycemc states. *Neurochem Int* 2006;48(6-7):616-622.
20. <http://www.mrui.uab.es/mrui/mruiHomePage.html>.
21. Naressi A, Couturier C, Devos JM, Janssen M, Mangeat C, de Beer R, Graveron-Demilly D. Java-based graphical user interface for the MRUI quantitation package. *Magnetic Resonance Materials in Physics Biology and Medicine* 2001;12(2-3):141-152.
22. Vanhamme L, van den Boogaart A, Van Huffel S. Improved method for accurate and efficient quantification of MRS data with use of prior knowledge. *J Magn Reson* 1997;129(1):35-43.
23. Choi IY, Tkac I, Ugurbil K, Gruetter R. Noninvasive measurements of [1-(13)C]glycogen concentrations and metabolism in rat brain in vivo. *J Neurochem* 1999;73(3):1300-1308.
24. Hendrich K, Garwood M, Merkle H, Ugurbil K. Spectroscopic Imaging Using Variable Angle Excitation from Adiabatic Plane-Rotation Pulses. *Magnetic Resonance in Medicine* 1991;19(2):496-501.

Figure Captions

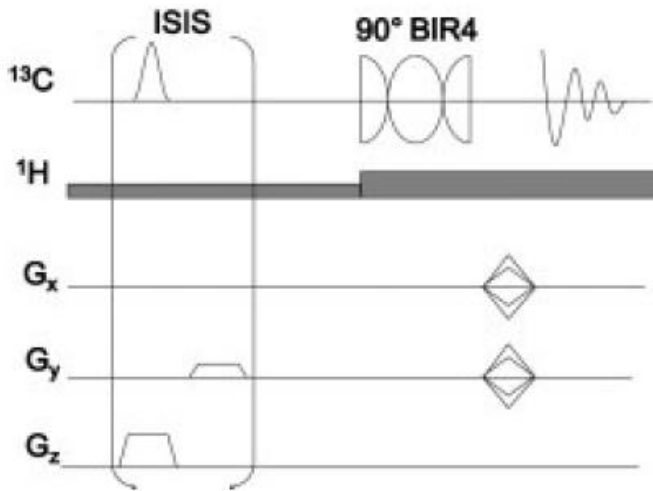


Figure 1. Diagram of the FOSSIL pulse sequence. The 90° BIR-4 pulse is preceded by a 1D ISIS module for slice selection. The time between the BIR-4 and the acquisition was 270 μ s, while the repetition time was 10 s for the phantom and 1 s for the rat.

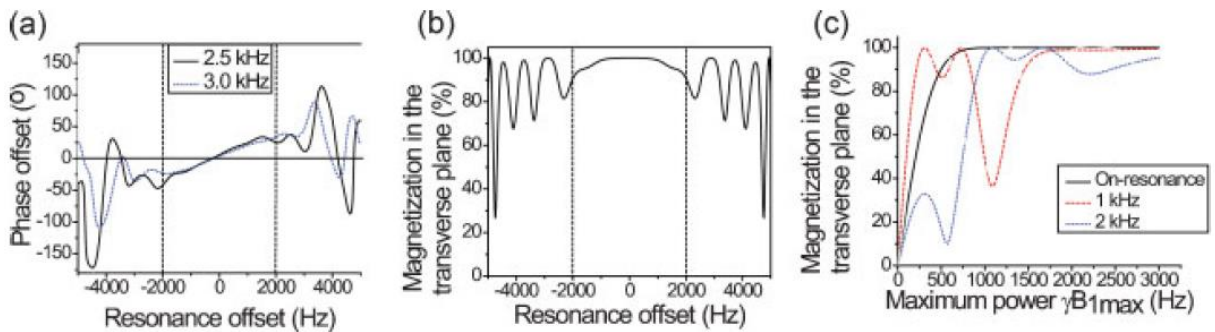


Figure 2. Simulated characteristics of a 3 ms 90° BIR-4 adiabatic pulse. a) Resonance offset versus phase offset at different values of γB_{1max} , with horizontal markers at 4 kHz bandwidth. Not far outside the bandwidth, the relation becomes incoherent. b) Resonance offset versus magnetization in the transverse plane at 2.5 kHz; outside a bandwidth of roughly 4.5 kHz the flip angle becomes incoherent.

c) Pulse power versus magnetization in the transverse plane. 2 kHz $\gamma B_{1\max}$ appears to be sufficient power for all offsets.

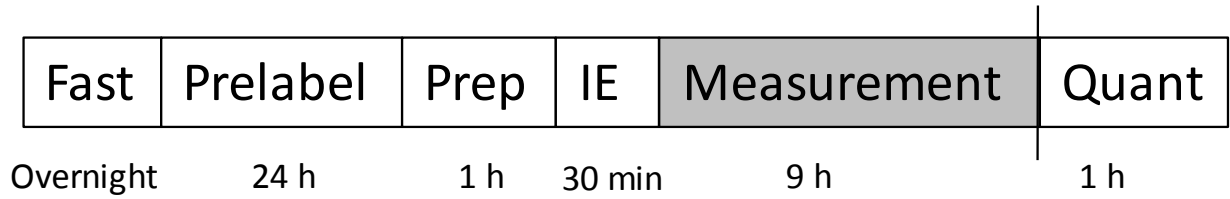


Figure 3. Overview of the experimental protocol and its timing. After fasting, the animal is prelabeled with C13 glucose, prepared for the study and inserted in the scanner, where its IE is determined. The main study itself then starts and lasts until sacrifice. After the study a phantom is inserted for absolute quantification purposes.

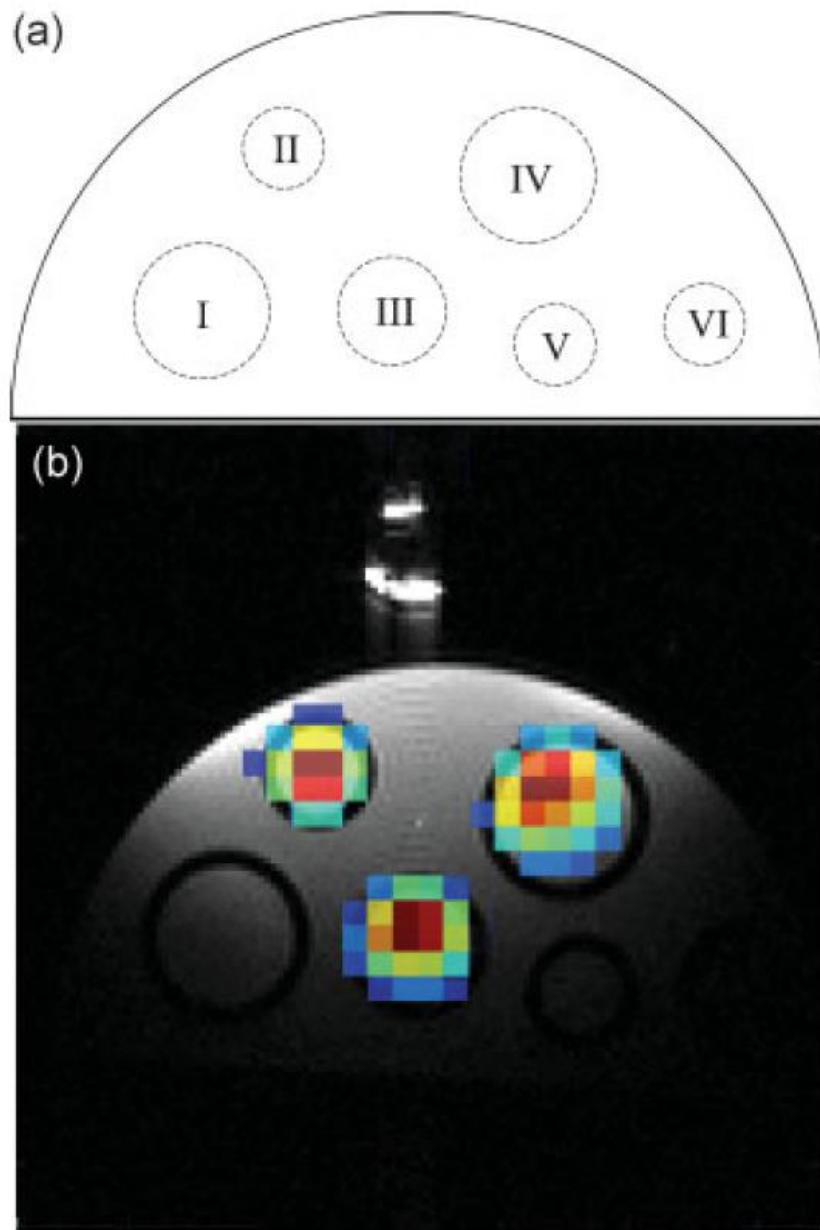


Figure 4. The localization capacity of the FSW sequence. a) Schematic drawing of the 30 mm wide and 52 mm long half-cylindrical localization phantom. The compartment diameters and solutions are: I. 6 mm filled with bicarbonate, II. 4 mm filled with formate, III. 5 mm filled with carbonate IV. 6 mm filled with acetate V. 4 mm filled with bicarbonate and VI. 4 mm filled with formate. The detection coil was placed on top of the phantom. b) Thresholded ^{13}C FSW color maps of the different resonances have

been projected on top of a ^1H gradient echo image. From left to right the color maps are formate, carbonate and acetate, all scaled to fit the same color range. The locations of the individual compartments can be seen in the gradient echo image, as can parts of the formic acid-filled bubble at the center of the coil.

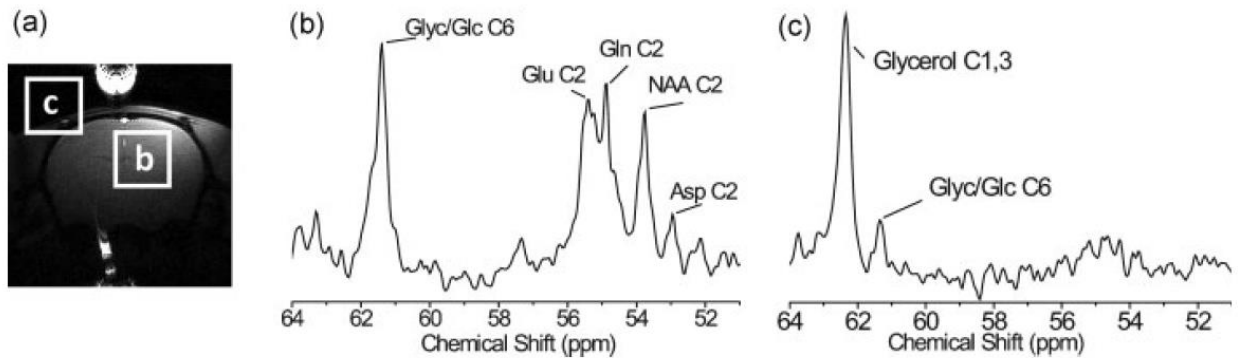


Figure 5. Demonstration of the FSW sequence localization capability. a) ^1H gradient echo image with the same FOV size as the FSW sequence ($22 \times 22 \text{ mm}^2$) and the positions of two windows indicated with white rectangles. b) Example of a localized spectrum in the brain. Note the presence of cerebral metabolites and the large glucose/glycogen peak. c) Localized spectrum outside the brain; in this case in the skin. Notice that the relative contribution of the glycerol is much bigger than that of glycogen and glucose C6, which still has a small presence due to the partial location of the voxel in the brain.

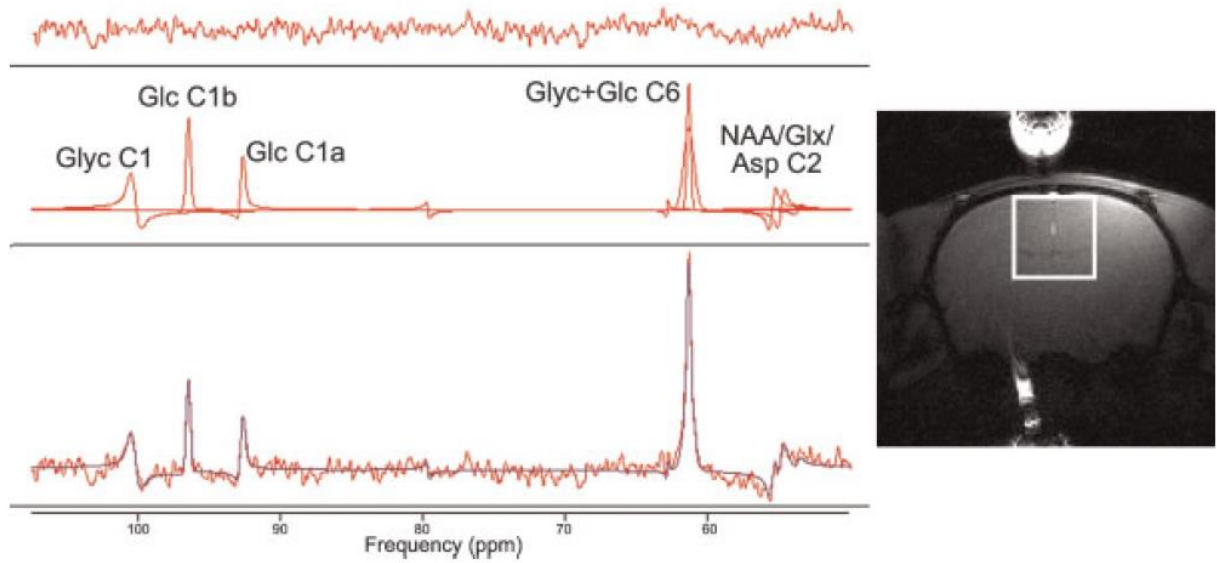


Figure 6. jMRUI fitting of a FSW brain spectrum after 6 h of infusion. Bottom: spectrum and fit. Middle: individual peaks with their names. Top: fit residual. Image: location of the window within the brain, with a formic acid phantom visible at the center of the detection coil.

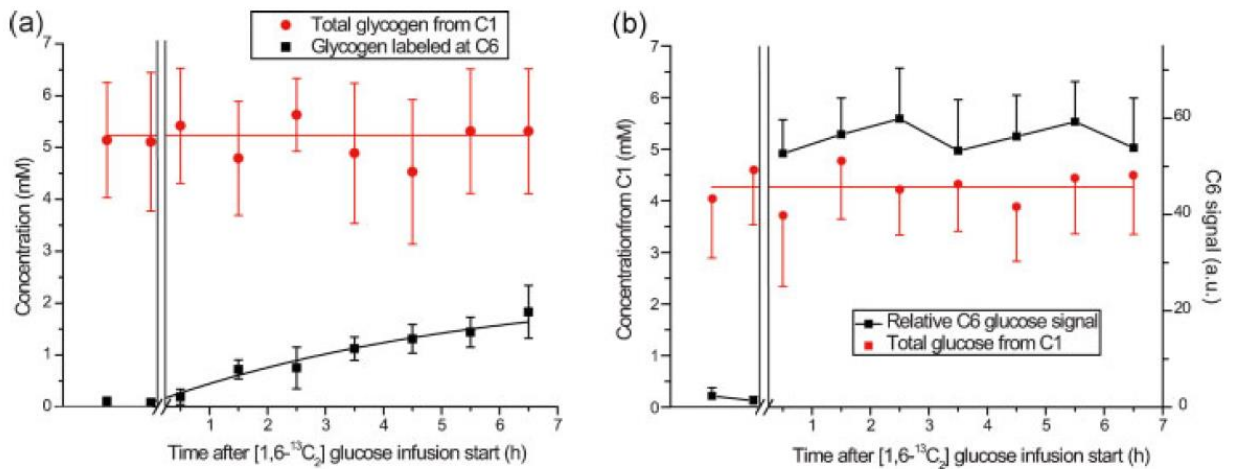


Figure 7. Time courses of the peaks. The two baseline FSW sets are represented as $t = -1$ and 0 . Later points are taken at the time halfway through their measurement, e.g. the first measurement after the C1,6 infusion start is taken as $t = 0.5$ h. Note that the Glc C6 is not quantified and thus has an arbitrary scale.